A simplified modal analysis of a single lap bonded joint using the macro-element technique

Benjamin Ordonneau, Eric Paroissien, Michel Salaün, Alejandro Benitez-Martin, Sébastien Schwartz, Julien Malrieu, Alexandre Guigue

A simplified modal analysis of a single lap bonded joint using the macro-element technique

Benjamin Ordonneau [a], Éric Paroissien [a,*], Michel Salaün [a], Alejandro Benitez-Martin [a], Sébastien Schwartz [a], Julien Malrieu [b], Alexandre Guigue [c]

[a] Institut Clément Ader (ICA), Université de Toulouse, ISAE-SUPAERO, INSA, IMT MINES ALBI, UTIII, CNRS, 3 Rue Caroline Aigle, 31400 Toulouse, France
[b] CETIM, 7 rue de la Presse, BP50802, 42952 Saint-Etienne Cedex 1, France
[c] DGA TA, 47 rue Saint-Jean, 31130 Balma, France

Keywords:
Modal analysis
Single-lap bonded joint
Functionally graded adhesive
Balanced joint
Unbalanced joint
Finite Element analysis
Macro-element

A B S T R A C T

Modal analyses are essential steps in structural design. Simple and quick numerical procedures and design tools for modal and dynamic analysis of bonded joints would be an attractive option to increase the efficiency of the design process in its early phases. This paper offers a simple and quick numerical tool dedicated to the modal analysis of single lap bonded joints with balanced and unbalanced adherends with various boundary conditions. Based on the macro-element technique developed with Taylor expansion in power series, this paper gives all the steps to develop the mass matrix associated with a macro-element. The mass matrix has been developed so far for 1D-bar and 1D-beam kinematic frameworks. The results obtained with the macro-element technique and a Finite Element analysis give similar results.

1. Introduction

a. Context

Adhesively bonded joints are an attractive option for structural design or repair thanks to their high mechanical performances (Hart-Smith, 1982; Kelly, 2006; da Silva et al., 2018). By joining the structures through a large contact area, the load transfer is distributed along the overlap and not located as it is for mechanical fasteners. The replacement of mechanical fastening by adhesive bonding tends to increase the strength-to-weight ratio of the structure. Strong and lightweight structures are a commercial advantage for transport industries and are perfectly in line with modern environmental policy.

The Finite Element (FE) method is commonly used to address the stress distribution in bonded joints and perform modal analyses. But due to the high ratio between the adherend thickness and the adhesive thickness, any simulation can be time-costly (Madenci, 2008). To address this, analytical analysis and simplified approaches have been developed to reduce the computing time or to be used as a preliminary design tool (Banea and da Silva, 2009).

For static analysis or non-linear analysis, many of these simplified approaches are analytical or semi-analytical. The analytical or semi-analytical solutions are dedicated to specific configurations under restrictive assumptions. Other methods are based on special FE which includes the adherend and the adhesive layer in a single element defined on the thickness of the joint, which avoid meshing through the thickness contrary to classical FE formulation (Carpenter and Barsoum, 1989; Andruet et al., 2001). These elements are developed from the strain–-stress equations of a bonded joint in 2D and 3D. Contrary to analytical approaches, the special FE approach needs a refined mesh, along the overlap, to converge. Contrary to the special FE approach mentioned before, a ME model does not need a refined mesh to converge. Thanks to the resolution of the governing equations of the joint, the exact shape functions of the element are computed. Then, a single ME represents the whole bonded overlap (Paroissien et al., 2013).

For modal analysis, some analytical approaches have been developed (Miles and Reihall, 1986; Rao and Crocker, 1990; Saito and Tani, 1984) but they also suffer a lack of versatility. Indeed, the analytical analysis is dedicated to a specific geometry and the number of computable vibration modes is limited. As modal analysis is an essential step in any structural design process, a simplified and adaptable methodology for the modal analysis of bonded joints could increase the efficiency of structural design in its early phases. In particular, for special FE, the mass matrix is missing to perform modal analysis.

* Corresponding author.
E-mail addresses: eric.paroissien@isae-supaero.fr, eric.paroissien@isae-supaero.fr (É. Paroissien).

https://doi.org/10.1016/j.ijsolstr.2022.111631

Nomenclature

symbols

A_j	extensional stiffness (N) of adherend j
C_u	vector of all the coefficients of all the TEPS
C_{u_1}	vector of the coefficients of the TEPS of the axial displacement of the upper adherend
C_{u_2}	vector of the coefficients of the TEPS of the axial displacement of the lower adherend
C_{v_1}	vector of the coefficients of the TEPS of the transverse displacement of the upper adherend
C_{v_2}	vector of the coefficients of the TEPS of the transverse displacement of the lower adherend
C_{θ_1}	vector of the coefficients of the TEPS of the rotation of the upper adherend
C_{θ_2}	vector of the coefficients of the TEPS of the rotation of the lower adherend
D_j	bending stiffness (N.mm^2) of adherend j
D_T	matrix of the recursive equation system with displacement boundary conditions
E_a	adhesive peel modulus (MPa)
G_a	adhesive shear modulus (MPa)
$E_{a,\min}$	minimal adhesive peel modulus (MPa)
$E_{a,\max}$	maximal adhesive peel modulus (MPa)
$G_{a,\min}$	minimal adhesive shear modulus (MPa)
$G_{a,\max}$	maximal adhesive shear modulus (MPa)
K	stiffness matrix
K_{BBa}	elementary stiffness matrix of a bonded-bar element
K_{BBe}	elementary stiffness matrix of a bonded-beam element
K_E	kinetic energy (J)
L	half-length (mm) of bonded overlap
L_{tot}	total length (mm) of bonded overlap
L_T	matrix with load boundary conditions
Lg_n	n-th Legendre polynomial
M_j	bending moment (N.mm) in adherend j around the z-direction
M	mass matrix
M_{BBa}	mass matrix of a ME in 1D bar kinematics
M_{BBe}	mass matrix of a ME in 1D beam kinematics
N	shape function matrix
N_{BBa}	shape function matrix of a ME in 1D bar kinematics
N_{BBe}	shape function matrix of a ME in 1D beam kinematics
N_j	normal force (N) in adherend j in the x-direction
N_u	number of terms in the series $u$after truncation
N_v	number of terms in the series $v$after truncation
P_n	nth Gauss-Legendre polynomial
$Q_{i,j,k,l}$	nodal axial force of node $i,j,k$and l
$R_{i,j,k,l}$	nodal shear force of node $i,j,k$and l
$S_{i,j,k,l}$	nodal moment force of node $i,j,k$and l
S	adhesive peel stress (MPa)
T	adhesive shear stress (MPa)
U_e	vector of the nodal displacements
V_j	shear force (N) in adherend j in the y-direction
b	width (mm) of the adherends
e_a	thickness (mm) of the adhesive layer
n_{FE}	number of Finite Elements used to mesh the overlap
n_{ME}	number of Macro-Elements used to mesh the overlap
$\dot{u}$	velocity field in the bonded joint
u_p	displacement (mm) of adherend j in the x-direction
v_p	displacement (mm) of adherend j in the y direction
w_i	weight of the Gauss-Legendre quadrature
θ_p	bending angle (rad) of the adherend $j$around the z-direction
ρ_{BBa}	density matrix (kg/m) of a bonded bar ME integrated over the cross section of the joint
ρ_{BBe}	density matrix (kg/m) of a bonded beam ME integrated over the cross section of the joint
ρ_1	density (kg/m^3) of the upper adherend
ρ_2	density (kg/m^3) of the lower adherend
ν_a	adhesive Poisson's ratio
ζ	dimensionless variable along the $x$axis
ζ_i	Gauss-Legendre integration points

abbreviations

BBa	bonded-bars
BBe	bonded-beams
FE	Finite Element
FGA	functionally graded adhesive
ME	macro-element
NF	natural frequency

b. ME overview

A ME is an element representing a whole bonded overlap joint in a single brick. Inspired by the FE method, a ME is characterised by its nodes and its stiffness matrix. Contrary to FE, the shape functions are derived from the governing equations of the system. It implies the mesh density of ME does not affect the stress distribution along the overlap. The accuracy of the results depends on the model and the resolution method used to derive the stiffness matrix and the shape functions. The modelling of a single lap bonded joint with a ME and 1D-bar/beam element is visible in Fig. 1. The nodes are all located at the neutral lines of the adherends. In this paper, the single lap joint is characterised by the adherend thicknesses e_1, e_2, the adhesive layer thickness e_a and the width b. The total length of the single lap joint is divided into three parts: the lengths of the outer adherends L_1, L_2 and the half length of the overlap L. The total length of the overlap is $L_{tot} = 2L$.

The first developed ME was dedicated to the static analysis of a homogeneous-adhesively-bonded joint in 1D-bar kinematics (Paroissien et al., 2007), using Arnovljevic's and Volkersen's 1D-bar bonded joint model (Arnovljevic, 1909; Volkersen, 1938). Based on Goland and Reissner's bending plate model, the ME has been extended to 1D-beam kinematics (Paroissien et al., 2007) and some procedures using the ME technique take into account non-linear adhesive behaviour (Lélias et al., 2015) or the progressive failure of the joint (Paroissien et al., 2013). Finally, using Tsaï et al.'s model, linear shear stress in the adherends is introduced into the equations to enrich the ME range (Tsaï et al., 1998).

The ME modelling is developed on the classical approaches based on beams on an elastic foundation for the simplified analysis of bonded joints (Paroissien et al., 2007). In 1D-bar kinematics, the adherend stress tensor is reduced to the normal stress component, which is constant through the thickness. In 1D-beam kinematics, the adherend stress tensor is reduced to the normal stress components, varying linearly through the thickness, and a shear component is chosen regarding the model used. The adhesive stress tensor is represented as an elastic foundation. In other words, the adhesive layer is regarded as a bed of springs coupling the kinematics of the adherends. The adhesive stress tensor is then reduced to only the shear stress component (shear and peel stress components) in 1D-bar (1D-beam) kinematics. The elastic foundation hypothesis implies the adhesive stresses are assumed to be constant through the adhesive thickness.

Three methods of resolution of differential equations have been used to develop all the different MEs. For the simplest configurations, the equations can be solved analytically. For multi-layered joints (Sekmen et al., 2020) or non-homogeneous joints (Paroissien et al., 2018; 2019), a

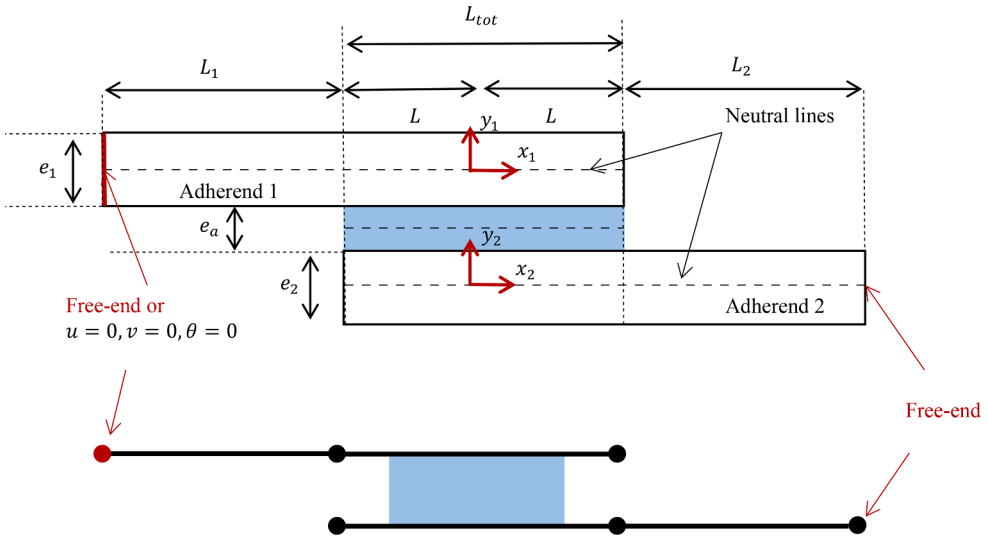

Fig. 1. Geometry parameters of the single lap bonded joint and its model with 1D-bar or beam FE and a ME for two sets of boundary conditions: free ends and clamped end - free end.

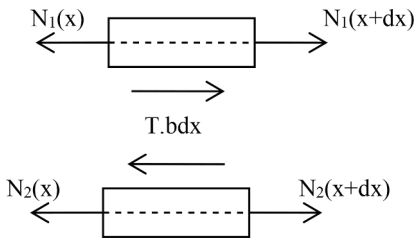

Fig. 2. Free body diagram of infinitesimal pieces included between x and $x+dx$ of both adherends in the overlap region under 1D-bar kinematics. Subscript 1 (2) refers to the upper (lower) adherend.

methodology based on exponential matrix has been introduced. This method allows the development of a ME with always the same methodology if the equations change due to a modification of model hypotheses. Contrary to the analytical resolution, the methodology based on exponential matrix implies the shape functions of the displacements and internal forces are not known anymore. They are only available at the nodes of the ME. To post-process the results at any abscissa, a dedicated mesh has to be used. The last resolution method makes use of TEPS. This method had been successfully used by Hart-Smith, in 1974, to address the stress distribution in a scarf joint (Hart-Smith, 1982). The use of TEPS led to the development of a ME dedicated to the static analysis of a joint with functionally graded properties (FGA) (Ordonneau et al., 2019). A single FGA ME represents the behaviour of a whole FGA bonded overlap and the shape functions can be easily computed to get the displacements of the adherends along the overlap. The accuracy of the results depends on the order of truncation of the power series.

c. Overview of the paper

In the present paper, the mass matrix associated with a ME, in 1D-bar and 1D-beam kinematics is presented. Its development follows the work (Ordonneau et al., 2019) in which the stiffness matrix of a ME is developed thanks to Taylor expansion power series (TEPS).

With the stiffness matrix from (Ordonneau et al., 2019) and the mass matrix presented here, modal analyses are performed on homogeneous and functionally graded adhesive (FGA) joints. The results given by the ME model are computed with MATLAB and compared with a PATRAN NASTRAN FE model.

Finally, the MATLAB codes used to do this work are provided as Supplementary Material for this paper.

2. Me mass matrix development

In this section, the development of the mass matrix of a ME, using TEPS, is presented in 1D-bar and 1D-beam kinematics. It is fully detailed in 1D –bar kinematics and only the main steps are given in 1D-beam kinematics. The details are available in Appendix A.

2.1. Governing equations

Before starting the development of the mass matrix of a ME, the hypotheses used to develop the stiffness matrix, in paper (Ordonneau et al., 2019) are presented. For both 1D-bar and 1D-beam cases, the adhesive layer thickness is assumed constant along the overlap. The materials have a linear elastic homogeneous behaviour. In 1D-bar kinematics, the constitutive equations of the adherends are:

$$N_p(x) = A_p \frac{du_p(x)}{dx}, p = 1, 2 \tag{1}$$

where u_p is the axial displacement of the adherend p, A_p the axial stiffness of the adherend p and the N_p the internal load in the adherend p. The constitutive equation of the adhesive layer is:

$$T(x) = \frac{G_a}{e_a}(u_2(x) - u_1(x)) \tag{2}$$

where G_a, the adhesive shear modulus and T the shear stress in the adhesive layer. According to Fig. 2, the local equilibrium of the adherends is expressed as:

$$\frac{dN_p(x)}{dx} = (-1)^p b T(x), p = 1, 2 \tag{3}$$

The constitutive equations associated with the joint in 1D-beam kinematics are visible in equation (4). The adherends are modelled as laminated Euler-Bernoulli beams. It is indicated that the methodology presented in this paper could be applied to any other beam model such as Timoshenko's or Tsaï et al's (Tsaï et al., 1998). The bending stiffness D_p of the adherend p is added. V_p is the shear force in the adherend p and M_p the bending moment.

The constitutive equations of the adherends are:

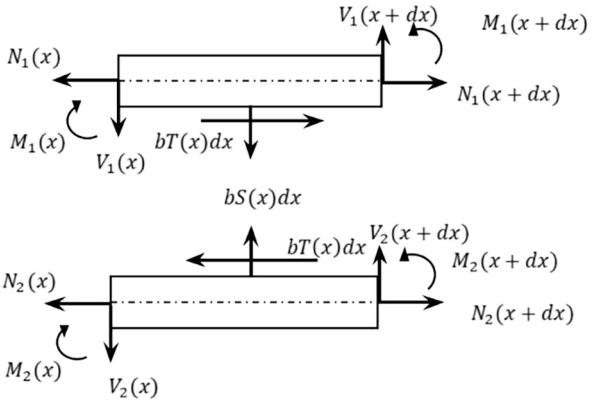

Fig. 3. Free body diagram of infinitesimal pieces included between × and x + dx of both adherends in the overlap region under 1D-beam kinematics. Subscript 1(2) refers to the upper (lower) adherend.

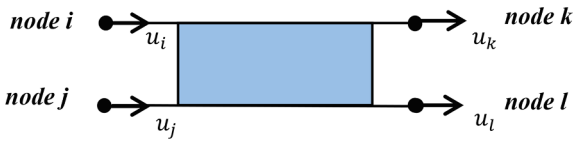

Fig. 4. Nodal boundary conditions in 1D bar kinematics.

$$\begin{cases} N_p(x) = A_p \dfrac{du_p(x)}{dx} \\ M_p(x) = D_p \dfrac{d\theta_p(x)}{dx}, p = 1,2 \\ \theta_p(x) = \dfrac{dv_p(x)}{dx} \end{cases} \tag{4}$$

where v_p the deflection and θ_p the bending angle of the adherend p. The constitutive equations of the adhesive layer now include the peel stress S and the adhesive peel modulus E_a. It reads:

$$\begin{cases} T = \dfrac{G_a}{e_a}\left(u_2 - u_1 - \dfrac{e_2}{2}\theta_2 - \dfrac{e_1}{2}\theta_1\right) \\ S = \dfrac{E_a}{e_a}(v_1 - v_2) \end{cases} \tag{5}$$

Finally, according to Fig. 3, the local equilibrium of the adherends is expressed by the following equations corresponding to Goland and Reissner's model:

$$\begin{cases} \dfrac{dN_p}{dx} = (-1)^p bT \\ \dfrac{dV_p}{dx} = (-1)^{p+1} bS \quad , p = 1,2 \\ \dfrac{dM_p}{dx} + V_p + \dfrac{be_p}{2}T = 0 \end{cases} \tag{6}$$

2.2. Mass matrix development in 1D bar kinematics

The derivation of the mass matrix in 1D-bar kinematics starts from the kinetic energy expression of the joint, say K_E, which reads:

$$K_E = \frac{1}{2}\iiint \rho \dot{u}(x,y)^2 dxdydz \tag{7}$$

where $\dot{u}$ is the velocity field in 1D-bar kinematics. In the case of an adhesively bonded joint, the kinetic energy is the sum of the kinetic energy of the two adherends. The local axis of each adherend is visible in Fig. 1.

$$K_E = \frac{1}{2}\iiint \rho_1 \dot{u_1}(x)^2 dxdydz + \frac{1}{2}\iiint \rho_2 \dot{u_2}(x)^2 dxdydz \tag{8}$$

After integration over the cross-section the kinetic energy becomes:

$$K_E = \frac{1}{2}\int_{-L}^{+L} \rho_1 b e_1 \dot{u_1}(x)^2 dx + \frac{1}{2}\int_{-L}^{+L} \rho_2 b e_2 \dot{u_2}(x)^2 dx \tag{9}$$

The kinetic energy is now written in a matrix form:

$$K_E = \frac{1}{2}\int_{-L}^{+L} [\dot{u_1}\dot{u_2}]^T \begin{bmatrix} e_1 b\rho_1 \& 0 \\ 0 \& e_2 b\rho_2 \end{bmatrix} \begin{bmatrix} \dot{u_1} \\ \dot{u_2} \end{bmatrix} dx \tag{10}$$

In the ME, the displacements are expressed with TEPS. More precisely, the expression of the displacement vector u is a function of $\zeta \in [1,-1]$ as the parameters of the series are chosen dimensionless (Ordonneau et al., 2019):

$$u = \begin{bmatrix} u_1(\zeta) \\ u_2(\zeta) \end{bmatrix} = \begin{bmatrix} [1\zeta\zeta^2 \cdots \zeta^{N_u-1}] C_{u_1} \\ [1\zeta\zeta^2 \cdots \zeta^{N_u-1}] C_{u_2} \end{bmatrix} \tag{11}$$

where N_u is the total number of coefficients in the series. C_{u_1} and C_{u_2} are the coefficient vectors of the series, with N_u lines and 1 row. The order of truncation is $N_u - 1$.

The use of TEPS to solve a system of differential equations (1) – (2) – (3) leads to a system with as many unknowns as coefficients of the series. Due to the order of the differential equations, four equations are missing in 1D-bar kinematics. Thus, four nodal boundary conditions are added to complete the system. In this paper, the matrix of the linear system associated with equations ((1)–(3)) and the nodal displacements equations, given in (Ordonneau et al., 2019), is called D_T and defined in such a way that:

$$D_T \begin{bmatrix} C_{u_1} \\ C_{u_2} \end{bmatrix} = \begin{bmatrix} [0]_{2(N_u-2)} \\ u_i \\ u_j \\ u_k \\ u_l \end{bmatrix} = \begin{bmatrix} [0]_{2(N_u-2)} \\ U_e \end{bmatrix} \tag{12}$$

where U_e is the nodal displacements vector, according to Fig. 4. The coefficients of the series are:

$$\begin{bmatrix} C_{u_1} \\ C_{u_2} \end{bmatrix} = D_T^{-1} \begin{bmatrix} [0]_{2(N_u-2)} \\ U_e \end{bmatrix} \tag{13}$$

The expression of the displacements becomes:

$$\begin{bmatrix} u_1(\zeta) \\ u_2(\zeta) \end{bmatrix} = \begin{bmatrix} [1\zeta\zeta^2 \cdots \zeta^{N_u-1}] \left[D_T^{-1} \begin{pmatrix} [0]_{2(N_u-2)} \\ U_e \end{pmatrix} \right]_{1 \cdots N_u} \\ [1\zeta\zeta^2 \cdots \zeta^{N_u-1}] \left[D_T^{-1} \begin{pmatrix} [0]_{2(N_u-2)} \\ U_e \end{pmatrix} \right]_{N_u+1 \cdots 2N_u} \end{bmatrix} \tag{14}$$

Only the columns of the matrix D_T^{-1} linked to the nodal displacement are kept:

$$\begin{bmatrix} u_1(\zeta) \\ u_2(\zeta) \end{bmatrix} = \begin{bmatrix} [1\zeta\zeta^2 \cdots \zeta^{N_u-1}] [D_T^{-1}]_{1 \cdots N_u \quad 2N_u-3 \cdots 2N_u} U_e \\ [1\zeta\zeta^2 \cdots \zeta^{N_u-1}] [D_T^{-1}]_{N_u+1 \cdots 2N_u \quad 2N_u-3 \cdots 2N_u} U_e \end{bmatrix} = N_{BBa}(\zeta) U_e \tag{15}$$

where N_{BBa} appears as the shape function matrix of the ME in 1D-bar kinematics. After the variable change $\zeta = \frac{x}{L}$ introduced in equation (10), the kinetic energy becomes:

$$K_E = \frac{1}{2}\int_{-1}^{+1} \dot{U}_e^T N_{BBa}^T(\zeta) \rho_{BBa} N_{BBa}(\zeta) \dot{U}_e L d\zeta \tag{16}$$

where ρ_{BBa} is the density matrix of the ME in 1D-beam kinematics:

Table 1
Mode shape of the first four non-zero NFs of a free-free end joint in 1D-bar and 1D-beam kinematics.

	1D-bar kinematics	1D-beam kinematics
NF n°1 (1st non-zero NF)		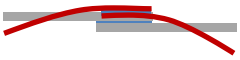
NF n°2 (2nd non-zero NF)	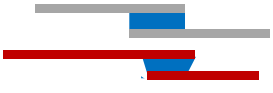	
NF n°3 (3rd non-zero NF)		
NF n°4 (4th non-zero NF)		

Table 2
Mode shape of the first four NFs of a clamped-free-end joint in 1D-bar and 1D-beam kinematics.

	1D-bar kinematics	1D-beam kinematics
NF n°1	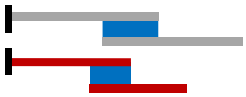	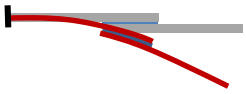
NF n°2		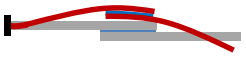
NF n°3		
NF n°4		

$$\rho_{BBa} = \begin{bmatrix} e_1 b\rho_1 \& 0 \\ 0 \& e_2 b\rho_2 \end{bmatrix} \tag{17}$$

The mass matrix M_{BBa} is identified as:

$$M_{BBa} = \int_{-1}^{1} N_{BBa}^{T}(\zeta)\rho_{BBa}N_{BBa}(\zeta)Ld\zeta \tag{18}$$

To integrate the matrix product, a Gauss-Legendre quadrature is used. The integral (18) becomes:

$$M_{BBa} = \sum_{i=0}^{N_u-1} Lw_i N_{BBa}^{T}(\zeta_i)\rho_{BBa}N_{BBa}(\zeta_i) \tag{19}$$

where ζ_i are the integration points, between [-1,1], and w_i the associated weights. The integration points are the roots of the orthogonal Legendre polynomial and the weights are computed with the formula:

$$w_i = \frac{2}{(1-\zeta_i^2)\left[P'_{N_u-1}(\zeta_i)\right]} \tag{20}$$

where P'_n is the first derivative of the $(N_u-1)^{th}$ Legendre polynomial (Abramowitz and Stegun, 1972).

2.3. Mass matrix development in 1D-beam kinematics

In this part, only the main steps to derive the mass matrix of the ME in 1D-beam kinematics are given. The kinetic energy in matrix form is:

$$K_E = \frac{1}{2}\int_{-L}^{+L} \begin{bmatrix} \dot{u_1}\dot{u_2}\dot{v_1}\dot{v_2}\dot{\theta_1}\dot{\theta_2} \end{bmatrix}^T \begin{bmatrix} \rho_1 & be_1 & 0 & 0 & 0 & 0 & 0 \\ 0 & \rho_2 & be_2 & 0 & 0 & 0 & 0 \\ 0 & 0 & \rho_1 & be_1 & 0 & 0 & 0 \\ 0 & 0 & 0 & \rho_2 & be_2 & 0 & 0 \\ 0 & 0 & 0 & 0 & \rho_1 & b\frac{{e_1}^3}{3} & 0 \\ 0 & 0 & 0 & 0 & 0 & \rho_2 & b\frac{{e_2}^3}{3} \end{bmatrix} \begin{bmatrix} \dot{u_1} \\ \dot{u_2} \\ \dot{v_1} \\ \dot{v_2} \\ \dot{\theta_1} \\ \dot{\theta_2} \end{bmatrix} dx \tag{21}$$

where $\dot{u_1}$,$\dot{u_2}$,$\dot{v_1}$,$\dot{v_2}$,$\dot{\theta_1}$ and $\dot{\theta_2}$ are the axial, transverse and angular velocities, respectively, of the upper adherend and the lower adherend. The displacement vector u, in 1D-beam kinematics, expressed with TEPS, is (Ordonneau et al., 2019):

$$u = \begin{bmatrix} u_1(\zeta) \\ u_2(\zeta) \\ v_1(\zeta) \\ v_2(\zeta) \\ \theta_1(\zeta) \\ \theta_2(\zeta) \end{bmatrix} = \begin{bmatrix} \left[1\zeta\zeta^2\cdots\zeta^{N_u-1}\right]C_{u_1} \\ \left[1\zeta\zeta^2\cdots\zeta^{N_u-1}\right]C_{u_2} \\ \left[1\zeta\zeta^2\cdots\zeta^{N_v-1}\right]C_{v_1} \\ \left[1\zeta\zeta^2\cdots\zeta^{N_v-1}\right]C_{v_2} \\ \left[1\frac{\zeta}{L}\frac{\zeta^2}{L^2}\cdots\frac{\zeta^{N_v-2}}{L^{N_v-2}}\right]C_{\theta_1} \\ \left[1\frac{\zeta}{L}\frac{\zeta^2}{L^2}\cdots\frac{\zeta^{N_v-2}}{L^{N_v-2}}\right]C_{\theta_2} \end{bmatrix} \tag{22}$$

where C_{u_1}, C_{u_2}, C_{v_1} and C_{v_2} are the column vectors of the coefficients of the series. C_{θ_1} and C_{θ_2} are the column vectors used to compute the rotations along the adherends. They are computed from the constitutive equation (4) and the vectors C_{v_1} and C_{v_2}. These coefficients are computed thanks to the following relationship:

$$D_T \begin{bmatrix} C_{u_1} \\ C_{u_2} \\ C_{v_1} \\ C_{v_2} \end{bmatrix} = \begin{bmatrix} [0]_{2N_u+2N_v-12} \\ u_i \\ u_j \\ u_k \\ u_l \\ v_i \\ v_j \\ v_k \\ v_l \\ \theta_i \\ \theta_j \\ \theta_k \\ \theta_l \end{bmatrix} = \begin{bmatrix} [0]_{2N_u+2N_v-12} \\ U_e \end{bmatrix} \tag{23}$$

where U_e is the nodal displacements vector in 1D-beam kinematics (according to Fig. 13 in Appendix A) and D_T is now the system matrix of the equations in 1D-beam kinematics.

The mass matrix of a ME in 1D-beam kinematic is then written:

$$M_{BBe} = \int_{-1}^{1} {N_{BBe}}^{T}\rho_{BBe}N_{BBe}Ld\zeta \tag{24}$$

where N_{BBe} and ρ_{BBe} are, respectively, the shape function matrix and the density matrix of the ME in 1D-bar kinematics. The matrix product is integrated with a Gauss-Legendre quadrature. All steps are detailed in Appendix A.

Table 3
Dimensions of the joint for the convergence study of the ME model.

e_1	e_1	e_a	b	$Ltot$	L_1	L_2
2 mm	2 mm	0.2 mm	25 mm	25 mm	55 mm	55 mm

Table 4
Materials of the adherends for the convergence study of the ME model.

	Young's modulus	Poisson's ratio	Density
Steel	210 GPa	0.3	8400 kg/m^3
Aluminum	70 GPa	0.29	2700 kg/m^3

3. ME modal analyses and convergence study

3.1. Natural frequency extraction

The natural frequencies (NFs) are derived from the eigenvalues of the stiffness matrix relatively to the mass matrix. They are defined as the square root of the eigenvalues, over two pi. Then, they are sorted out in ascending order.

The mode shapes associated with each NF are presented in Table 1 and Table 2. The original shape of the joint is sketched in grey and the mode shape in red. In 1D-bar kinematics, the original shape and the mode shape are separated to better visualize the deformation of the adhesive and the axial extension or compression of the adherends. In 1D-beam kinematics, the two shapes are superimposed to visualise the deflection of the joint.

In 1D-bar kinematics, the behaviour of the adherends can be confusing as the structure only deforms in one direction. This behaviour is briefly described here. Considering Table 1, for the 1st non-zero NF, both upper and lower adherends are in compression. For the 2nd, the upper adherend is in extension and the lower adherend is in compression. For the 3rd, both upper and lower outer adherends are in compression while both upper and lower adherends in the overlap region are in extension. For the last, the upper outer adherend is in compression and the upper adherend in the overlap region is in extension while the lower adherend in the overlap region is in compression and the lower outer adherend is in extension.

Considering now Table 2, for NF n°1, both upper and lower adherends are in compression. For NF n°2, the upper adherend is in extension while the lower adherend is in compression. For NF n°3, the upper outer adherend is in extension, the lower outer adherend is in compression while both upper and lower adherend in the overlap region are neither extended nor compressed. Finally, for NF n°4, both upper and lower outer adherends are in extension while both upper and lower adherends in the overlap region are in compression. The extension or compression is not constant along the adherends which can lead to a different deformation of the adhesive at each end of the joint, as visible in the figures in Table 1 and Table 2.

In 1D-beam kinematics, the behaviour of the adherends can be easily understood from the mode shapes in Table 2 and is not detailed.

3.2. Convergence of the natural frequencies

The convergence of the eigenvalues is linked to the number of degrees of freedom of the system. MEs are used to mesh the overlap and bar or beam elements are used to mesh the outer adherends. A convergence study is performed on the NFs as a function of the number of MEs, nb_{ME}, used to mesh the lap joint. The same number of elements nb_{ME} is used to mesh the overlap and to mesh each of the outer adherends with bar or beam elements. The total number of elements used to mesh the whole structure is thus $3nb_{ME}$.

Two homogeneous isotropic materials are used for the tests. Balanced (steel-steel) and unbalanced (steel-aluminium) joints are considered for both 1D-bar kinematics and 1D-beam kinematics and free-free end and clamped-free end boundary conditions are applied. In this paper, the terms balanced and unbalanced are used to describe joints with similar or dissimilar adherends. The dimensions and materials of the adherends are given in Table 3 and Table 4.

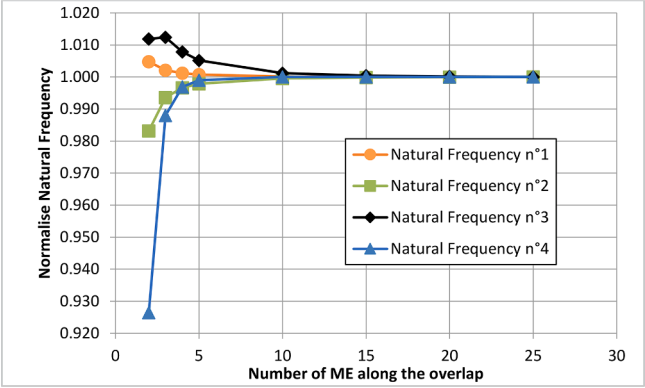

Fig. 5. Convergence of the first four non-zero NFs of a free-free end balanced joint in 1D-bar kinematics – ME model.

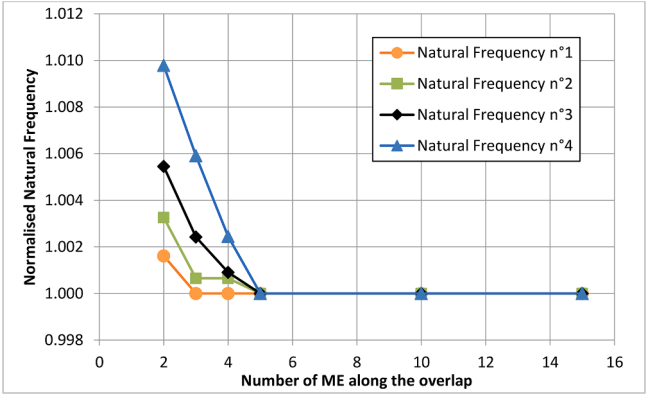

Fig. 6. Convergence of the first four non-zero NFs of a free-free end balanced joint in 1D-beam kinematics.

In 1D-bar kinematics, the shear modulus of the adhesive is chosen as $G_a = 1000MPa$ and the adhesive layer thickness is $0.1mm$. In 1D-beam kinematics, the adhesive peel modulus is chosen as $E_a = 2000MPa$ and the shear modulus of the adhesive, computed from the adhesive peel modulus, is $G_a = 740MPa$. The adhesive layer thickness is 0.2 mm.

According to (Ordonneau et al., 2019), the stiffness matrix of a homogeneous ME converges for a truncation of the series at $N_u \geq 10$ in 1D-bar kinematics and $N_u \geq 40$ at 1D-beam kinematics. Then, the coefficients of the series are considered as converged and so is the mass matrix.

The convergence of the first four non-zero NFs of a balanced joint with free-free end boundary conditions is presented in Fig. 5 in 1D-bar and Fig. 6 in 1D-beam kinematic frameworks. On the graphs, each NF is normalised by the NF obtained with the more refined mesh and is presented as a function of the number of ME, nb_{ME}, along the overlap. The convergence studies for clamped-free end joints and unbalanced joints show similar behaviour and so are not presented.

In 1D-bar kinematics, the first four NFs converge at a number of ME along the overlap $nb_{ME} = 20$. In 1D-beam kinematics, the first four NFs converge at a number of ME along the overlap $nb_{ME} = 5$.

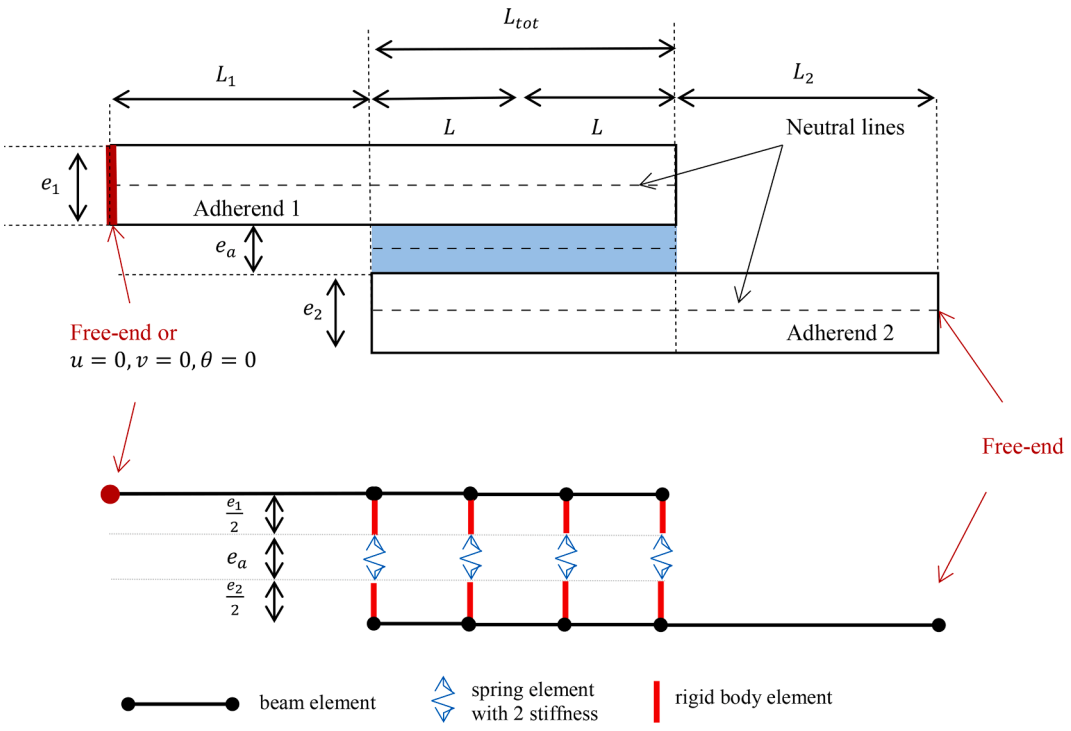

Fig. 7. FE model of the single lap bonded joint in 1D-beam kinematics.

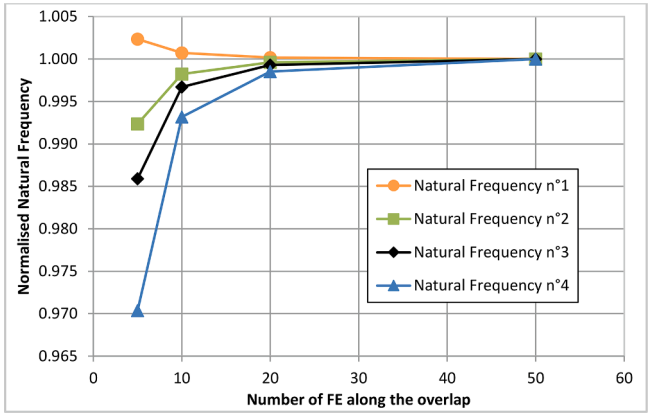

Fig. 8. Convergence of the first four non-zero NFs for a free-free end balanced joint in 1D-bar kinematics – FE model.

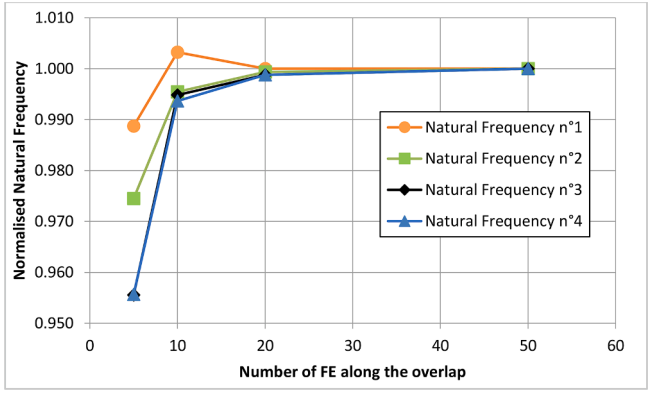

Fig. 9. Convergence study of the first four non-zero NFs for a free-free end balanced joint in 1D beam kinematics – FE model.

Table 5
Results and comparison between the ME model and the FE model in 1D-bar kinematics.

1D-BAR KINEMATICS			
Balanced Joint			
Free-free end configuration	ME	FE	Error
NF n° 1	19,640	19,640	0.00%
NF n° 2	32,478	32,480	−0.01%
NF n° 3	58,196	58,167	0.05%
NF n° 4	68,936	68,915	0.03%
Clamped-free end configuration			
NF n° 1	8724	8724	0.00%
NF n° 2	26,499	26,499	0.00%
NF n° 3	44,857	44,851	0.01%
NF n° 4	63,533	63,507	0.04%
Unbalanced Joint			
Free-free end configuration	ME	FE	Error
NF n° 1	20,466	20,466	0.00%
NF n° 2	32,533	32,535	−0.01%
NF n° 3	59,622	59,601	0.05%
NF n° 4	69,568	69,549	0.03%
Clamped-free end configuration			
NF n° 1	11,682	11,682	0.00%
NF n° 2	24,935	24,936	−0.00%
NF n° 3	46,175	46,169	0.01%
NF n° 4	65,341	65,317	0.04%

4. Validation

4.1. Description of the FE model

Two FE models have been designed according to the hypothesis used to develop the ME. The first one is using 1D-bar and the second one is using 1D-beam kinematics.

Table 6
Results and comparison between the ME model and the FE model in 1D-beam kinematics.

1D-BEAM KINEMATICS			
Balanced Joint			
Free-free end configuration	ME	FE	Error
NF n° 1	621	620	0.16%
NF n° 2	1533	1530	0.20%
NF n° 3	3302	3284	0.55%
NF n° 4	4907	4874	0.68%
Clamped-free end configuration			
NF n° 1	87	87	0.00%
NF n° 2	569	568	0.18%
NF n° 3	1525	1521	0.26%
NF n° 4	3312	3290	0.67%
Unbalanced Joint			
Free-free end configuration	ME	FE	Error
NF n° 1	611	609	0.33%
NF n° 2	1561	1561	0.00%
NF n° 3	3329	3309	0.60%
NF n° 4	4909	4895	0.29%
Clamped-free end configuration			
NF n° 1	136	136	0.00%
NF n° 2	594	592	0.34%
NF n° 3	1543	1546	−0.19%
NF n° 4	3334	3311	0.69%

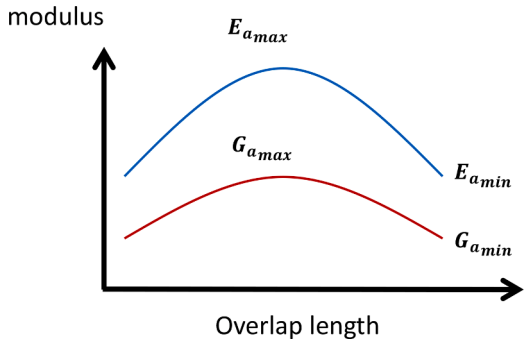

Fig. 10. Typical parabolic graduation of the adhesive properties along the overlap.

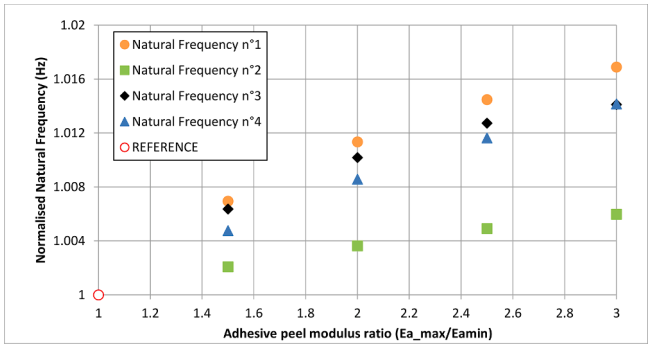

Fig. 11. Normalised NFs of the FGA joint − 1D-bar kinematics.

Based on the work presented in (Paroissien et al., 2018), the FE models developed are spring-based. The adherends are modelled with bar or beam elements with cubic interpolation functions and the nodes are located on the neutral lines. The adhesive layer is represented with shear springs only in 1D-bar kinematics and shear and peel springs in 1D-beam kinematics. In 1D-bar kinematics, the end nodes of the springs are attached to the bar elements. In 1D beam kinematics, the end nodes of the spring elements are located at the actual interface of the adherends. The connection between the nodes of the neutral lines and the nodes of the interface is made with rigid body elements, according to the Euler-Bernoulli beam theory. A scheme of the FE model in 1D-beam kinematics is shown in Fig. 7. The stiffness of the shear and peel springs are defined such as (Dechwayukul et al., 2003):

$$k_{shear}(x) = m(x)\frac{L}{nb_{FE}}b\frac{G_a(x)}{e_a} \tag{25}$$

$$k_{peel}(x) = m(x)\frac{L}{nb_{FE}}b\frac{E_a(x)}{e_a} \tag{26}$$

With $m(0 < x < L) = 1$ and $m(x = 0) = m(x = L) = \frac{1}{2}$. nb_{FE} is the number of elements along the overlap, G_a is the adhesive shear modulus and E_a its adhesive peel modulus, characterizing the transverse tensile behaviour of the adhesive layer (Ordonneau et al., 2019). As the accuracy of such a model has already been shown in (Paroissien et al., 2018), only the convergence of the results of modal analyses is presented here.

4.2. Convergence study

The two cases presented in this section are the same as in section 3. For all dimensions and materials, refer to Table 3 and Table 4. The structure is meshed with the same number of elements nb_{FE} along the overlap and along each adherend. In 1D-bar kinematics, a single spring is used between the nodes of the bar element along the overlap. The total number of elements is $5nb_{FE} + 1$. In 1D-beam kinematics, two spring elements are used to connect the nodes of the rigid elements along the overlap. The total number of elements is $8nb_{FE} + 4$.

The convergence of the NFs computed with the FE model are presented in Fig. 8 and Fig. 9. The rigid body modes are not presented and each NF is normalised by its converged value.

The convergence is achieved for a number of FE along the overlap $\mathbf{nb_{FE}} = 20$ for the configurations presented in.

Fig. 8 and Fig. 9. The same observation has been made for all other configurations. For the comparisons in the following section, this number of elements will be used.

4.3. Comparison between the ME model and the FE model

In this section, the comparison between the ME model and the FE model is presented. The NFs in Table 5 and Table 6 are considered converged. It corresponds to a mesh with $nb_{ME} = 20$ for the ME model in 1D-bar and $nb_{ME} = 5$ for the ME model in 1D-beam kinematics, and a mesh with $nb_{FE} = 20$ for the FE model in 1D-bar and 1D-beam kinematics. The error is defined as follows.$Error = \left(\frac{ME_{value}}{FE_{value}} - 1\right)*100$

All errors are below 0.1% in 1D-bar kinematics and most of the errors are below 0.5% in 1D-beam kinematics. The small error on the NFs validates the use of the ME technique to perform modal analyses on adhesively bonded structures.

These results are obtained with a ME model with 60 elements in total in 1D-bar kinematics and 15 elements in total in 1D-beam kinematics. The FE model is made of 101 elements in 1D-bar kinematics (20 elements in each outer adherend, 20 elements in each adherend along the overlap and 21 spring elements along the overlap) and 164 elements in 1D-beam kinematics (20 elements in each outer adherend, 20 elements in each adherend along the overlap and 42 spring elements along the overlap and 42 rigid elements along the overlap). In (Paroissien et al., 2013), a time computation comparison was made between a ME and a detailed 3D FE model of a single-lap bonded joint involving nonlinear material behavior. It was found that the computation time associated with the ME model was 50 times lower than the 3D FE model. It was

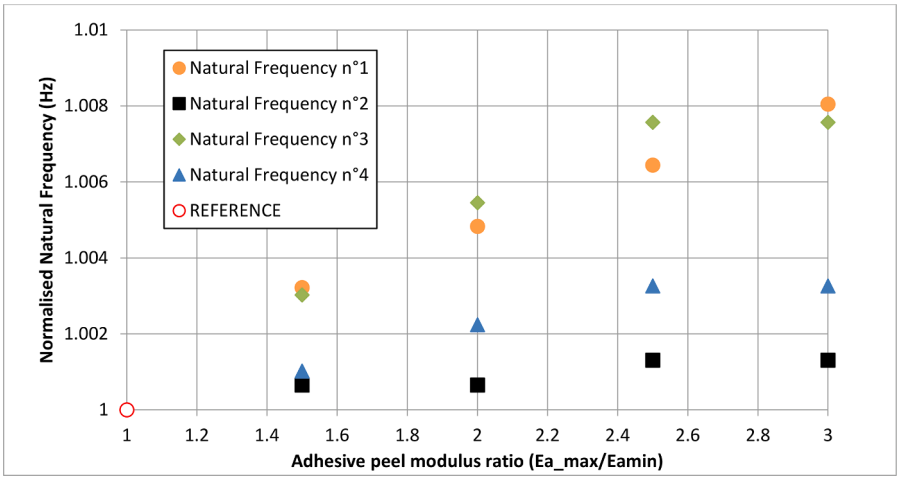

Fig. 12. Normalised NFs of the FGA joint – 1D-beam kinematics.

shown the stress distribution along the adhesive mid-layer provided by the model was in a close agreement with the one by the 3D FE model. Of course, due the classical set of simplified hypotheses used, the ME model is not able to represent for the boundary layer effect in the adhesive at the very ends of the overlap leading to difference in adhesive peak location and values. A detailed comparison is provided in (Paroissien et al., 2019). Moreover, it is obvious that the 3D FE model provides more detailed information such the mechanical behavior at overlap ends. In this paper, the computation time between the ME model and the simplified FE model was measured for both about 1 s on a common laptop. Firstly, this comparison has to be considered with precautions. The ME model was implemented without any intention of computation time performance optimization, since the only objective of this comparison between the ME and FE models was to validate the methodologies and associated code. Secondly, it could be thought that, for the elementary test case presented in this paper, there is no advantage to use the ME model. As stated in the introduction section of this paper, several ME formulation methodologies have been developed. A research effort is currently in progress on two other formulation methodologies by the way. The objective of these research actions is to enrich the ME modelling. By nature, the ME gathered the assumed simplified physics of the adhesive and adherends. To be more representative for the physical reality, the way to alleviate the restrictions associated with the simplified hypotheses is under investigation through the formulation methodologies. As an example shown in (Paroissien et al., 2018; 2019), it is easy to investigate the effect of the choice of simplified hypotheses on the accuracy of results provided by the ME model. Another example is related to the simulation of the progressive failure of the adhesive layer through the cohesive zone approach, enriching the ME model (Lélias et al., 2015). To suitably dissipate the energy, a refined mesh has to be used. When using FE model based on solid element, the number of degrees of freedom is quickly increased since the mesh refinement is required in the three directions to insure the quality of the FE model, contrary to the ME model for which only one direction is concerned (Lélias et al., 2015). The number of degrees of freedom is directly linked to the computation time. Another interest which can be underlined is common to simplified analysis: the ME model can be easily integrated in optimization process to explore the design space with the advantage to take into account for the variation of hypotheses. Similarly, the ME model is an attractive candidate in the frame of reliability-based design process. Thirdly, the comparison should not be restricted to time computation and accuracy only. Indeed, when using the FE method with commercial FE software, the preprocessing time to design, create and justify a FE model cannot be neglected as well as the cost associated with the information system required. For example, the creation of a well-designed FE model involving a graduation of adhesive properties

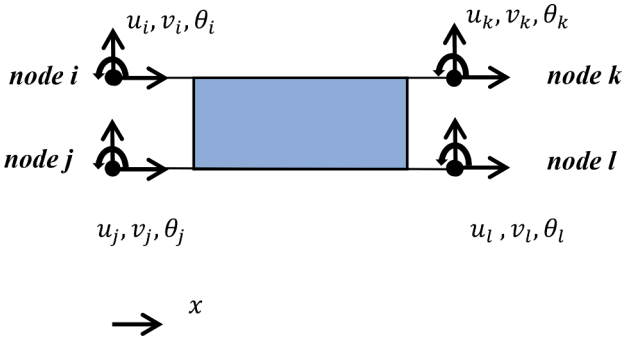

Fig. 13. Nodal boundary condition diagram in 1D beam kinematics.

(Paroissien et al., 2019) is time consuming, even for a simplified FE model such as used in the next section of this paper.

5. Natural frequency of a functionally graded adhesive (Fga) joint

The use of an FGA allows increasing the strength of a joint without modification of its geometry. This part aims to investigate the influence of the graduation of the adhesive on the NFs of a joint. The next section presents the procedure to compute the ME mass matrix of an FGA joint. Then, modal analyses are performed on free-free end FGA joints.

5.1. Mass matrix of an FGA ME

According to section 2.2 and 2.3, the mass matrix depends on the shape functions of the element. The shape functions of an FA ME are computed the same way as for a homogeneous ME, for both 1D-bar and 1D-beam kinematics. They are identified from the expression of the displacements of the adherends along the overlap. Similarly to equations (13) and (33), the coefficients of the series are expressed with the matrix of the system associated with an FGA joint, which is detailed in (Ordonneau et al., 2019).

As the adhesive layer and its properties are not taken into account in the density matrix, the integral leading to the mass matrix is not modified in the case of an FGA joint.

The procedure to compute the mass matrix is then the same for an FGA joint or a homogeneous joint.

5.2. Modal analyses of an FGA joint

5.2.1. Definition of the FGA properties

The FGA is defined by the graduation of the adhesive properties along the overlap. Here, it has been chosen to consider a parabolic graduation of the stiffness along the overlap. The adhesive peel modulus and the adhesive shear modulus are computed at any normalised abscissa with the formulae:

$$E_a(\zeta) = E_{amax} - (E_{amax} - E_{amin})(\zeta^2 - 1)$$

$$G_a(\zeta) = G_{amax} - (G_{amax} - G_{amin})(\zeta^2 - 1) \quad (27)$$

where E_{amax} and E_{amin} are the maximum and minimum values of the adhesive peel modulus and G_{amax} and G_{amin} are the maximum and minimum values of the adhesive shear modulus. This distribution is shown Fig. 10.

Four cases have been considered and compared to a reference case. The adhesive peel modulus of the reference case is chosen as constant along the overlap, with $E_a = 2000MPa$. The four different tested cases have a minimum adhesive modulus $E_{amin} = 2000MPa$ and the maximum adhesive moduli are: $E_{amax} = 3000MPa$ for the first case, $E_{amax} = 4000MPa$ for the second case, $E_{amax} = 5000MPa$ for the third case and $E_{amax} = 6000MPa$ for the last case. The adhesive Poisson's ratio is chosen to be constant along the overlap and is $\nu_a = 0.35$. The adhesive shear moduli are computed from the adhesive peel moduli. The geometrical parameters of the joint are given in Table 3 and the adherends are made of steel. The adhesive thickness is 0.2 mm.

5.2.2. Results of the modal analyses of an FGA joint

To compute the NFs of the FGA joint, the stiffness matrix developed in (Ordonneau et al., 2019) and the mass matrix of an FGA joint presented in this paper are used. The joint is meshed as presented in section 3.2 and according to (Ordonneau et al., 2019), the order of truncation of the series has been increased to $N_u = 15$ in 1D-bar kinematics and $N_u = 40$ in 1D-beam kinematics due to the FGA. Free-free end boundary condition is applied. The evolution of the first four NFs as a function of the graduation is presented in Fig. 11 and Fig. 12. The NFs are normalised by the NF obtained with the reference case and presented as a function of the ratio between the maximum and minimum adhesive peel moduli.

The values of the NFs and the normalised NFs are given in Appendix B. The graduation of the adhesive properties leads to a slight increase of the NFs of the joint, in both 1D-bar and 1D-beam kinematics. At the extreme, the NFs are increased by around 2%.

Finally, compared to a joint with homogeneous adhesive properties, the graduation of adhesive properties does not significantly change the NF, while reducing the maximal adhesive stresses (Paroissien et al., 2018; 2019; Ordonneau et al., 2019; Carbas et al., 2014; Stein et al., 2016; 2017).

6. Conclusion

In this paper, modal analyses of a single-lap-bonded joint are performed in 1D-bar and 1D-beam kinematics thanks to the ME technique.

All the mathematical details to compute the mass matrix associated with a ME from its shape functions are given. The shape functions are derived from the development of a ME thanks to TEPS (Ordonneau et al., 2019).

The mass matrix for a homogeneous joint has been validated with a FE model. This FE model is a spring-based model to be under the hypotheses used to develop both stiffness and mass matrix of the ME.

The validation is done on various configurations. A set of two boundary conditions are used with similar and different adherends. The discrepancy between the NFs computed with the ME model and with the spring-based FE model, used as a reference solution, is below half per cent in most of the studied cases.

The mass matrix of a ME associated with an FGA joint is used to investigate the influence of a parabolic graduation of the adhesive properties on the NFs. This study is done on a balanced joint and with two different boundary conditions. It appears the graduation increases the NFs between 0.5% and 2%.

The use of the ME to model the joint allows computing easily any number of NFs for various configurations of single-lap joints.

Finally, the validation of the mass matrix presented in this paper currently allows the application of the ME modelling in the frame rapid dynamic analysis, such as the test of bonded joints with the split-Hopkinson pressure bar or composite bonded repairs under impact loading.

Declaration of Competing Interest

The authors declare that they have no known competing financial interests or personal relationships that could have appeared to influence the work reported in this paper.

Acknowledgement

The authors are grateful to the French institutions Centre Technique des Industries Mécaniques (CETIM) and Direction Générale de l'Armement (DGA) for their financial support.

Appendix A:. Development of the mass matrix of a ME in 1D-beam kinematics

In this appendix, all the steps and mathematical details to develop the mass matrix of the ME in 1D-beam kinematics are presented. As for 1D-bar kinematics, the derivation of the mass matrix M_{BBe} in 1D-beam kinematics starts from the kinetic energy. The energy due to the translation of the joint and its rotation are separated.

$$K_E = \frac{1}{2}\iiint \rho_1 \left(\dot{u_1}(x)^2 + \dot{v_1}(x)^2\right) dV + \frac{1}{2}\iiint \rho_1 \left(-y_2\dot{\theta_1}(x)\right)^2 dV + \frac{1}{2}\iiint \rho_2 \left(\dot{u_2}(x)^2 + \dot{v_2}(x)^2\right) dxdydz + \frac{1}{2}\iiint \rho_2 \left(-y_2\dot{\theta_2}(x)\right)^2 dxdydz \quad (28)$$

After integration over the cross-section (the local axis of each adherend is visible in Fig. 1), the kinetic energy becomes:

$$K_E = \frac{1}{2}\int_{-L}^{+L} \rho_1 be_1 \left(\dot{u_1}(x)^2 + \dot{v_1}(x)^2\right) dx + \frac{1}{2}\int_{-L}^{+L} \rho_2 be_2 \left(\dot{u_2}(x)^2 + \dot{v_2}(x)^2\right) dx + \frac{1}{2}\int_{-L}^{+L} \rho_1 b\frac{1}{3}e_1{}^3\dot{\theta}_1(x)^2 dx + \frac{1}{2}\int_{-L}^{+L} \rho_2 b\frac{1}{3}e_2{}^3\dot{\theta}_2(x)^2 dx \quad (29)$$

The kinetic energy is now written in a matrix form:

$$K_E = \frac{1}{2}\int_{-L}^{+L} \begin{bmatrix} \dot{u}_1 \dot{u}_2 \dot{v}_1 \dot{v}_2 \dot{\theta}_1 \dot{\theta}_2 \end{bmatrix} \begin{bmatrix} \rho_1 & be_1 & 0 & 0 & 0 & 0 & 0 \\ 0 & \rho_2 & be_2 & 0 & 0 & 0 & 0 \\ 0 & 0 & \rho_1 & be_1 & 0 & 0 & 0 \\ 0 & 0 & 0 & \rho_2 & be_2 & 0 & 0 \\ 0 & 0 & 0 & 0 & \rho_1 & b\frac{{e_1}^3}{3} & 0 \\ 0 & 0 & 0 & 0 & 0 & \rho_2 & b\frac{{e_2}^3}{3} \end{bmatrix} \begin{bmatrix} \dot{u}_1 \\ \dot{u}_2 \\ \dot{v}_1 \\ \dot{v}_2 \\ \dot{\theta}_1 \\ \dot{\theta}_2 \end{bmatrix} dx \tag{30}$$

The expression of the displacement vector u, expressed with TEPS, is a function of $\zeta \in [1, -1]$ as the parameters of the series are chosen dimensionless (Paroissien et al., 2007):

$$u = \begin{bmatrix} u_1(\zeta) \\ u_2(\zeta) \\ v_1(\zeta) \\ v_2(\zeta) \\ \theta_1(\zeta) \\ \theta_2(\zeta) \end{bmatrix} = \begin{bmatrix} \begin{bmatrix} \begin{bmatrix} 1\zeta\zeta^2 \cdots \zeta^{N_u-1} \end{bmatrix} C_{u_1} \\ \begin{bmatrix} 1\zeta\zeta^2 \cdots \zeta^{N_u-1} \end{bmatrix} C_{u_2} \\ \begin{bmatrix} 1\zeta\zeta^2 \cdots \zeta^{N_u-1} \end{bmatrix} C_{v_1} \\ \begin{bmatrix} 1\zeta\zeta^2 \cdots \zeta^{N_v-1} \end{bmatrix} C_{v_2} \\ \begin{bmatrix} 1\frac{\zeta}{L}\frac{\zeta^2}{L^2} \cdots \frac{\zeta^{N_v-2}}{L^{N_v-2}} \end{bmatrix} C_{\theta_1} \\ \begin{bmatrix} 1\frac{\zeta}{L}\frac{\zeta^2}{L^2} \cdots \frac{\zeta^{N_v-2}}{L^{N_v-2}} \end{bmatrix} C_{\theta_2} \end{bmatrix} \end{bmatrix} \tag{31}$$

where C_{u_1}, C_{u_2}, C_{v_1} and C_{v_2} are the column vectors of the coefficients of the series. C_{θ_1} and C_{θ_2} are the column vectors used to compute the rotations along the adherends. They are computed from the constitutive equation (4) and the vectors C_{v_1} and C_{v_2}. In 1D-beam kinematics, these coefficient vectors are solutions of the following linear system:

$$D_T \begin{bmatrix} C_{u_1} \\ C_{u_2} \\ C_{v_1} \\ C_{v_2} \end{bmatrix} = \begin{bmatrix} [0]_{2N_u+2Nv-12} \\ u_i \\ u_j \\ u_k \\ u_l \\ v_i \\ v_j \\ v_k \\ v_l \\ \theta_i \\ \theta_j \\ \theta_k \\ \theta_l \end{bmatrix} = \begin{bmatrix} [0]_{2N_u+2Nv-12} \\ U_e \end{bmatrix} \tag{32}$$

where U_e is the nodal displacements vector in 1D-beam kinematics, according to Fig. 13, and N_u is the total number of coefficients in the series u_1 and u_2 and N_v is the total number of coefficients in the series v_1 and v_2. The coefficients of the series are:

$$\begin{bmatrix} C_{u_1} \\ C_{u_2} \\ C_{v_1} \\ C_{v_2} \end{bmatrix} = D_T^{-1} \begin{bmatrix} [0]_{2N_u+2Nv-12} \\ U_e \end{bmatrix} \tag{33}$$

The displacements becomes:

$$\begin{bmatrix} u_1(\zeta) \\ u_2(\zeta) \\ v_1(\zeta) \\ v_2(\zeta) \\ \theta_1(\zeta) \\ \theta_2(\zeta) \end{bmatrix} = \begin{bmatrix} \left[1\zeta\zeta^2\cdots\zeta^{N_u-1}\right]\left[D_T^{-1}\begin{pmatrix}[0]_{2N_u+2Nv-12}\\ U_e\end{pmatrix}\right]_{1\cdots N_u} \\ \left[1\zeta\zeta^2\cdots\zeta^{N_u-1}\right]\left[D_T^{-1}\begin{pmatrix}[0]_{2N_u+2Nv-12}\\ U_e\end{pmatrix}\right]_{N_u+1\cdots 2N_u} \\ \left[1\zeta\zeta^2\cdots\zeta^{N_v-1}\right]\left[D_T^{-1}\begin{pmatrix}[0]_{2N_u+2Nv-12}\\ U_e\end{pmatrix}\right]_{2N_u+1\cdots 2N_u+N_v} \\ \left[1\zeta\zeta^2\cdots\zeta^{N_v-1}\right]\left[D_T^{-1}\begin{pmatrix}[0]_{2N_u+2Nv-12}\\ U_e\end{pmatrix}\right]_{2N_u+N_v+1\cdots 2N_u+2N_v} \\ \left[1\frac{\zeta}{L}\frac{\zeta^2}{L^2}\cdots\frac{\zeta^{N_v-2}}{L^{N_v-2}}\right]\left[D_T^{-1}\begin{pmatrix}[0]_{2N_u+2Nv-12}\\ U_e\end{pmatrix}\right]_{2N_u+2\cdots 2N_u+N_v} \\ \left[1\frac{\zeta}{L}\frac{\zeta^2}{L^2}\cdots\frac{\zeta^{N_v-2}}{L^{N_v-2}}\right]\left[D_T^{-1}\begin{pmatrix}[0]_{2N_u+2Nv-12}\\ U_e\end{pmatrix}\right]_{2N_u+N_v+2\cdots 2N_u+2N_v} \end{bmatrix} \tag{34}$$

Only the last 12 columns of the matrix D_T^{-1} are kept:

$$\begin{bmatrix} u_1(\zeta) \\ u_2(\zeta) \\ v_1(\zeta) \\ v_2(\zeta) \\ \theta_1(\zeta) \\ \theta_2(\zeta) \end{bmatrix} = \begin{bmatrix} \left[1\zeta\zeta^2\cdots\zeta^{N_u-1}\right]\left[D_T^{-1}\right]_{2N_u+2N_v-11\cdots 2N_u+2N_v}^{1\cdots N_u} U_e \\ \left[1\zeta\zeta^2\cdots\zeta^{N_u-1}\right]\left[D_T^{-1}\right]_{2N_u+2N_v-11\cdots 2N_u+2N_v}^{N_u+1\cdots 2N_u} U_e \\ \left[1\zeta\zeta^2\cdots\zeta^{N_u-1}\right]\left[D_T^{-1}\right]_{2N_u+2N_v-11\cdots 2N_u+2N_v}^{2N_u+1\cdots 2N_u+N_v} U_e \\ \left[1\zeta\zeta^2\cdots\zeta^{N_u-1}\right]\left[D_T^{-1}\right]_{2N_u+2N_v-11\cdots 2N_u+2N_v}^{2N_u+N_v+1\cdots 2N_u+2N_v} U_e \\ \left[1\frac{\zeta}{L}\frac{\zeta^2}{L^2}\cdots\frac{\zeta^{N_v-2}}{L^{N_v-2}}\right]\left[D_T^{-1}\right]_{2N_u+2N_v-11\cdots 2N_u+2N_v}^{2N_u+2\cdots 2N_u+N_v} U_e \\ \left[1\frac{\zeta}{L}\frac{\zeta^2}{L^2}\cdots\frac{\zeta^{N_v-2}}{L^{N_v-2}}\right]\left[D_T^{-1}\right]_{2N_u+2N_v-11\cdots 2N_u+2N_v}^{2N_u+N_v+2\cdots 2N_u+2N_v} U_e \end{bmatrix} = N_{BBe}(\zeta)U_e \tag{35}$$

where N_{BBe} is the shape function matrix of the ME in 1D-beam kinematics. After the variable change $= \frac{x}{L}$, the kinetic energy becomes:

$$K_E = \frac{1}{2}\int_{-1}^{+1} \dot{U}_e^T N_{BBe}^T(\zeta)^T \rho_{BBe} N_{BBe}(\zeta)\dot{U}_e L d\zeta \tag{36}$$

with ρ_{BBe} is the density matrix of ME in 1D-beam kinematics:

$$\rho_{BBe} = \begin{bmatrix} \rho_1 & be_1 & 0 & 0 & 0 & 0 & 0 \\ 0 & \rho_2 & be_2 & 0 & 0 & 0 & 0 \\ 0 & 0 & \rho_1 & be_1 & 0 & 0 & 0 \\ 0 & 0 & 0 & \rho_2 & be_2 & 0 & 0 \\ 0 & 0 & 0 & 0 & \rho_1 & b\frac{{e_1}^3}{3} & 0 \\ 0 & 0 & 0 & 0 & 0 & \rho_2 & b\frac{{e_2}^3}{3} \end{bmatrix} \tag{37}$$

The mass matrix M_{BBe} is identified as:

$$M_{BBe} = \int_{-1}^{1} N_{BBe}^T(\zeta)\rho_{BBe} N_{BBe}(\zeta) L d\zeta \tag{38}$$

To integrate the matrix product, a Gauss-Legendre quadrature is used.

Appendix B:. Table of the NFs of an FGA joint

In this appendix, the NFs of an FGA joint computed with the ME are presented in 1D-bar and 1D-beam kinematics in. Table 7. The normalised NFs, associated with the graphs visible in Fig. 11 and Fig. 12 are presented in Table 8.

Table 7
NF of the FGA joint as a function of the maximum adhesive peel modulus.

	1D-BAR KINEMATICS				1D-BEAM KINEMATICS			
	Free Free				Free Free			
Ea max	NF1	NF1	NF1	NF1	NF1			
3000	19,259	32,182	57,317	67,507	625	1535	3325	4925
4000	19,343	32,232	57,534	67,763	628	1537	3341	4938
5000	19,403	32,273	57,679	67,969	630	1538	3353	4948
6000	19,449	32,307	57,758	68,139	632	1539	3363	4956
REFERENCE	**19,130**	**32,104**	**57,016**	**67,211**	**621**	**1533**	**3302**	**4907**

Table 8
Normalised NF of the FGA joint as a function of the maximum adhesive peel modulus.

	1D-BAR KINEMATICS				1D-BEAM KINEMATICS			
	Free Free				Free Free			
Ea max	NF1	NF1	NF1	NF1	NF1	NF2	NF3	NF4
3000	1.0070	1.0021	1.0064	1.0048	1.0032	1.0007	1.0030	1.0010
4000	1.0113	1.0036	1.0102	1.0086	1.0048	1.0007	1.0055	1.0022
5000	1.0145	1.0049	1.0127	1.0116	1.0064	1.0013	1.0079	1.0033
6000	1.0169	1.0060	1.0141	1.0142	1.0081	1.0013	1.0091	1.0043

Appendix C. Supplementary data

Supplementary data to this article can be found online at https://doi.org/10.1016/j.ijsolstr.2022.111631.

References

Hart-Smith, LJ, 1982. Design methodology for bonded-bolted composite joints. Technical Report, AFWAL-TR-81-3154, Douglas Aircraft Company, Long Beach, California.

Kelly, G., 2006. Quasi-static strength and fatigue life of hybrid (bonded/bolted) composite single-lap joints. Compos. Struct. 72, 119–129. https://doi.org/10.1016/j.compstruct.2004.11.002.

da Silva, L.F.M., Öschner, A., Adams, R.D., 2018. Editors). Handbook of Adhesion Technology (2 volumes), 2nd edition. Springer, Heidelberg, Germany.

Madenci, B., 2008. Analysis of bolted bonded composite SLJ under combined in plane and transverse loading. Compos. Struct. 88, 579–594. https://doi.org/10.1016/j.compstruct.2008.06.003.

Banea, M.D., da Silva, L.F.M., 2009. Adhesively bonded joints in composite materials: an overview. Proc. Inst. Mech. Eng. L 223, 1–18. https://doi.org/10.1243/14644207JMDA219.

Carpenter, W.C., Barsoum, R., 1989. Two finite elements for modeling the adhesive in bonded configurations. J. Adhes. 30, 25–46. https://doi.org/10.1080/00218468908048192.

Andruet, R.H., Dillard, D.A., Holzer, S.M., 2001. Two-and three-dimensional geometrical nonlinear finite elements for analysis of adhesive joints. Int. J. Adhes. Adhes. 21, 17–34. https://doi.org/10.1016/S0143-7496(00)00024-5.

Paroissien, E., Gaubert, F., Da Veiga, A., Lachaud, F., 2013. Elasto-plastic analysis of bonded joints with macro-elements. J. Adhes. Sci. Technol. 27, 1464–1498. https://doi.org/10.1080/01694243.2012.745053.

Miles, R.N., Reihall, P.G., 1986. An analytical model for the vibration of laminated beams including the effects of both shear and thickness deformation in the adhesive layer. J. Vib. Acoust. 108, 56–64. https://doi.org/10.1115/1.3269304.

Rao, M.D., Crocker, M.J., 1990. Analytical and experimental study of the vibration of bonded beams with a lip joint. J. Vib. and Acoust. 12, 444–445. https://doi.org/10.1115/1.2930127.

Saito, H., Tani, H., 1984. Vibration of bonded beams with a single-lap adhesive joint. J. Sound Vib. 92, 299–309. https://doi.org/10.1016/0022-460X(84)90563-7.

Paroissien, E., Sartor, M., Huet, J., 2007. In: Hybrid (bolted/bonded) joints applied to aeronautic parts: Analytical one-dimensional models of a single-lap joint. Springer, Dordrecht, The Netherlands, pp. 95–110. https://doi.org/10.1007/978-1-4020-6761-7_7.

Arnovljevic, I., 1909. Das Verteilungsgesetz der Tiefspannungen in axial beanspruchten Verbundstaben. Z.F. Archund-Ing-Wesen, 55, 415-418.

Volkersen, O., 1938. Die Nietkraftverteilung in Zugbeanspruchten Nietverbindungen mit konstanten Laschenquerschnitten. Luftfahrforschung 15 (24), 41–47.

Paroissien, E., Sartor, M., Huet, J., Lachaud, F., 2007. Analytical two-dimensional model of a hybrid (bolted/bonded) single-lap joint. J. Aircraft 44 (2), 573–582. https://doi.org/10.2514/1.24452.

Lélias, G., Paroissien, E., Lachaud, F., Morlier, J., Schwartz, S., Gavoille, C., 2015. An extended semi-analytical formulation for fast and reliable stress analysis of adhesively bonded joints. Int. J Solids Struct. 62, 18–39. https://doi.org/10.1016/j.ijsolstr.2014.12.027.

Paroissien, E., Gaubert, F., Da Veiga, A., Lachaud, F., 2013. Elasto-Plastic analysis of bonded joints with macro-elements. J. Adhes. Sci. Technol. 27 (13), 1464–1498. https://doi.org/10.1080/01694243.2012.745053.

Tsaï, M.Y., Oplinger, D.W., Morton, J., 1998. Improved theoretical solutions for adhesive lap joints. J. Adhes. Sci. Technol. 35, 1163–1185. https://doi.org/10.1016/S0020-7683(97)00097-8.

Sekmen, K., Paroissien, E., Lachaud, F., 2020. Simplified stress analysis of multilayered adhesively bonded structures. Int. J. Adhes. Adhes. 97, 102497 https://doi.org/10.1016/j.ijadhadh.2019.102497.

Paroissien, E., da Silva, L.F.M., Lachaud, F., 2018. Simplified stress analysis of functionally graded single-lap joints subjected to combined thermal and mechanical loads. Compos. Struct. 203, 85–100. https://doi.org/10.1016/j.compstruct.2018.07.015.

Paroissien, E., Lachaud, F., da Silva, L.F.M., Seddiki, S., 2019. A comparison between macro-element and finite element solutions for the stress analysis of functionally graded single-lap joints. Compos. Struct. 215, 331–350. https://doi.org/10.1016/j.compstruct.2019.02.070.

Ordonneau, B., Paroissien, E., Salaun, M., Malrieu, J., Guigue, A., Schwartz, S., 2019. A methodology of the macro-element stiffness matrix for the stress analysis of a lap joint with functionally graded adhesive properties. Int. J. Adhes. Adhes. 97, 102505 https://doi.org/10.1016/j.ijadhadh.2019.102505.

Abramowitz, M., Stegun, I.A, 1972. Handbook of Mathematical Functions With Formulas, Graphs and Mathematical Tables. Corrected version, 887.

Dechwayukul, C., Rubin, C.A., Hahn, G.T., 2003. Analysis of the effects of thin sealant layers in aircraft structural joints. AIAA J. 41, 2216–2228. https://doi.org/10.2514/2.6814.

Carbas, R.J.C., da Silva, L.F.M., Madureira, M.L., Critchlow, G.W., 2014. Modelling of functionally graded adhesive joints. J. Adhesion 90 (8), 698–716. https://doi.org/10.1080/00218464.2013.834255.

Stein, N., Weißgraeber, P., Becker, W., 2016. Stress solution for functionally graded adhesive joints. Int. J. Solids Struct. 97–98, 300–311. https://doi.org/10.1016/j.ijsolstr.2016.07.019.

Stein, N., Felger, J., Becker, W., 2017. Analytical models for functionally graded adhesive joints: a comparative study. Int. J. Adhes. Adhes. 76, 70–82. https://doi.org/10.1016/j.ijadhadh.2017.02.001.